Estradiol Regulates Energy Balance by Ameliorating Hypothalamic Ceramide-Induced ER Stress

I Gonzalez-Garcia, C Contreras, A Estevez-Salguero, F Ruiz-Pino, B Colsh, I Pensado, L Linares-Pose, E Rial-Pensado, Pbm de Morentin, J Ferno, et al.

Article

Cell Reports

Estradiol Regulates Energy Balance by Ameliorating Hypothalamic Ceramide-Induced ER Stress

Graphical Abstract

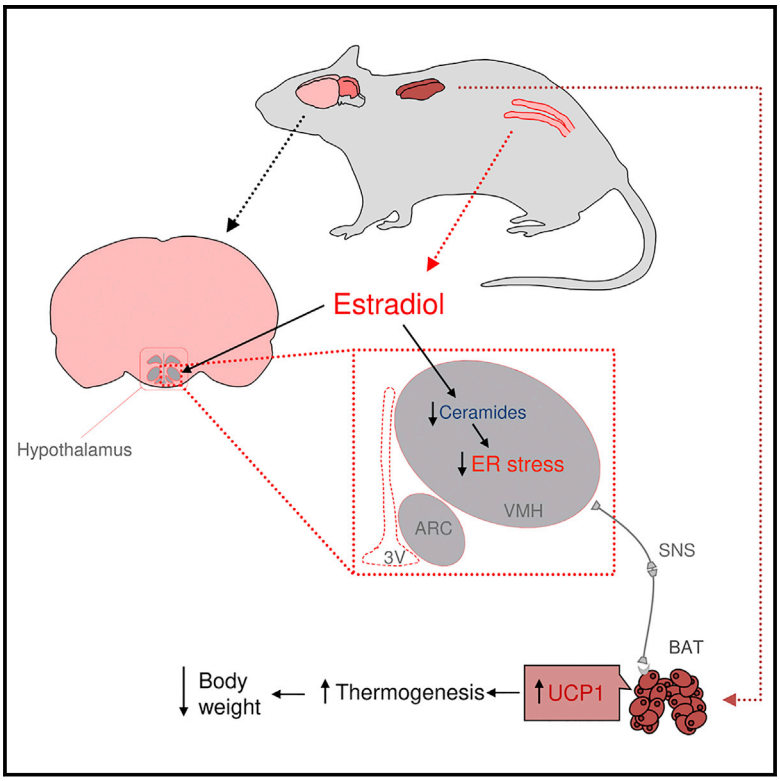

Highlights

- Central E2 regulates BAT thermogenesis via the sympathetic nervous system
- Central E2 reduces hypothalamic ceramides and ER stress
- Hypothalamic ceramides/ER stress mediate E2 actions on BAT

Authors

Ismael González-García,
Cristina Contreras,
Ánxela Estévez-Salguero, ...,
Christophe Magnan,
Manuel Tena-Sempere, Miguel López

Correspondence

m.lopez@usc.es

In Brief

González-García et al. demonstrate that estradiol (E2) acts in a precise area of the hypothalamus, named the ventromedial nucleus (VMH), to regulate brown fat thermogenesis. The actions of E2 are mediated by modulation of hypothalamic ceramides and ER stress.

González-García et al., 2018, Cell Reports *25*, 413–423
October 9, 2018
https://doi.org/10.1016/j.celrep.2018.09.038

CellPress

Cell Reports
Article

Estradiol Regulates Energy Balance by Ameliorating Hypothalamic Ceramide-Induced ER Stress

Ismael González-García,[1,2] Cristina Contreras,[1,2] Ánxela Estévez-Salguero,[1,2] Francisco Ruíz-Pino,[2,3,4] Benoit Colsh,[5] Iván Pensado,[1,2] Laura Liñares-Pose,[1,2] Eva Rial-Pensado,[1,2] Pablo B. Martínez de Morentin,[1,2] Johan Fernø,[6] Carlos Diéguez,[1,2] Rubén Nogueiras,[1,2] Hervé Le Stunff,[7,8] Christophe Magnan,[8] Manuel Tena-Sempere,[2,3,4,9] and Miguel López[1,2,10,*]

[1]Department of Physiology, CiMUS, University of Santiago de Compostela-Instituto de Investigación Sanitaria, Santiago de Compostela, 15782, Spain
[2]CIBER Fisiopatología de la Obesidad y Nutrición (CIBERobn), Santiago de Compostela, 15706, Spain
[3]Department of Cell Biology, Physiology, and Immunology, University of Córdoba, Córdoba, 14004, Spain
[4]Instituto Maimónides de Investigación Biomédica (IMIBIC)/Hospital Reina Sofía, Córdoba, 14004, Spain
[5]CEA-Centre d'Etude de Saclay, Laboratoire d'étude du Métabolisme des Médicaments, Gif-sur-Yvette, France
[6]Hormone Laboratory, Haukeland University Hospital, Bergen, 5021, Norway
[7]Paris-Saclay Institute of Neuroscience, CNRS UMR 9197, Université Paris-Sud, University Paris Saclay, Orsay 91405 Cedex, France
[8]Unité de Biologie Fonctionnelle et Adaptative, CNRS UMR 8251, Université Paris Diderot, Sorbonne Paris Cité, Paris, 75205, France
[9]FiDiPro Program, Research Centre for Integrative Physiology and Pharmacology, University of Turku, Kiinamyllynkatu 10, 20520 Turku, Finland
[10]Lead Contact
*Correspondence: m.lopez@usc.es
https://doi.org/10.1016/j.celrep.2018.09.038

SUMMARY

Compelling evidence has shown that, besides its putative effect on the regulation of the gonadal axis, estradiol (E2) exerts a dichotomic effect on the hypothalamus to regulate food intake and energy expenditure. The anorectic effect of E2 is mainly mediated by its action on the arcuate nucleus (ARC), whereas its effects on brown adipose tissue (BAT) thermogenesis occur in the ventromedial nucleus (VMH). Here, we demonstrate that central E2 decreases hypothalamic ceramide levels and endoplasmic reticulum (ER) stress. Pharmacological or genetic blockade of ceramide synthesis and amelioration of ER stress selectively occurring in the VMH recapitulate the effect of E2, leading to increased BAT thermogenesis, weight loss, and metabolic improvement. These findings demonstrate that E2 regulation of ceramide-induced hypothalamic lipotoxicity and ER stress is an important determinant of energy balance, suggesting that dysregulation of this mechanism may underlie some changes in energy homeostasis seen in females.

INTRODUCTION

One of the most interesting and least understood aspects of energy balance modulation is gender dimorphism. Although some common mechanisms control energy balance in both males and females, elevated levels of ovarian steroids deeply affect metabolic networks in females (Mauvais-Jarvis et al., 2013, 2017; Palmer and Clegg, 2015; Mauvais-Jarvis, 2015; Morselli et al., 2016; López and Tena-Sempere, 2017). For example, diminished levels of estradiol (E2) after ovarian insufficiency of any etiology, including physiological (menopause) or surgical (ovariectomy [OVX]), are associated with hyperphagia, reduced energy expenditure, and weight gain (Mauvais-Jarvis et al., 2013, 2017; Palmer and Clegg, 2015; Mauvais-Jarvis, 2015; Morselli et al., 2016; López and Tena-Sempere, 2017). E2 replacement in these conditions precludes or reverts OVX-induced obesity by reducing energy intake and elevating energy expenditure; in keeping with this, E2 replacement also prevents metabolic complications, such as glucose intolerance and diabetes. (Mauvais-Jarvis et al., 2013, 2017; Palmer and Clegg, 2015; Mauvais-Jarvis, 2015; Morselli et al., 2016; López and Tena-Sempere, 2017). Although these beneficial effects of E2 were assumed to be mostly exerted at the peripheral level, recently gleaned data have shown that, to a large extent, they are exerted at the hypothalamus.

E2 directly acts on the CNS to modulate energy balance (López and Tena-Sempere, 2015, 2017). Estrogen receptors (ERs) are widely expressed throughout the brain, particularly in hypothalamic sites, such as the arcuate (ARC), ventromedial (VMH), and paraventricular (PVH) nuclei, as well as the preoptic (POA) and lateral (LHA) hypothalamic areas (Simerly et al., 1990; Simonian and Herbison, 1997; Voisin et al., 1997; Osterlund et al., 1998; Merchenthaler et al., 2004), all having critical roles in the regulation of energy metabolism (Schneeberger et al., 2014; Scott et al., 2014; Magnan et al., 2015; López et al., 2016; Cui et al., 2017). Several lines of evidence have shown that E2 exerts a nucleus-specific action in the hypothalamus to modulate energy homeostasis. Thus, while most of the effects of E2 on feeding occur in proopiomelanocortin (POMC) neurons in the ARC (Xu et al., 2011), E2 within the VMH modulates brown adipose tissue (BAT) thermogenesis (Musatov et al., 2007; Xu et al., 2011; Martínez de Morentin et al., 2014, 2015). However,

the exact molecular mechanism by which E2 exerts its actions in this nucleus remains unknown.

Current evidence has pointed to hypothalamic endoplasmic reticulum (ER) stress as a central pathophysiological mechanism leading to insulin and leptin resistance and subsequently to obesity (Zhang et al., 2008; Martínez de Morentin and López, 2010; Ozcan et al., 2009; Schneeberger et al., 2013). It also has been shown that central ceramide-induced lipotoxicity affects energy balance (Ramírez et al., 2013; Picard et al., 2013; Turpin et al., 2014; Contreras et al., 2014; Magnan et al., 2015). In the hypothalamus, elevated ceramide concentration elicits ER stress, leading to weight gain, insulin resistance, hepatic steatosis, decreased sympathetic tone, and BAT thermogenesis (Contreras et al., 2014, 2017). Notably, the central action of ceramides can be reversed by decreasing hypothalamic ER stress, resulting in increased BAT thermogenesis and browning of white adipose tissue (WAT), which ultimately ameliorates obesity (Contreras et al., 2014, 2017). It also has been reported that peripheral E2 treatment reduces serum ceramide concentration in OVX rats (Vinayavekhin et al., 2016). However, despite this evidence, it is currently unknown (1) whether ovarian estrogens modulate hypothalamic ceramide-induced lipotoxicity, and, more importantly, (2) whether impairment of this mechanism may be the cause of obesity in conditions of estrogen deficiency. Therefore, in this study we aim to determine the importance of hypothalamic ceramides and ER stress on the central effects of E2 on energy homeostasis.

RESULTS

Central E2 Inhibits Hypothalamic Ceramide-Induced Lipotoxicity and ER Stress

OVX rats gained significantly more weight 15 days after the procedure (sham: 12.7 ± 2.54 g; OVX: 48.63 ± 2.38 g; $p < 0.001$) and developed a marked hyperphagia (sham: 16.1 ± 0.42 g; OVX: 18.25 ± 0.40 g after 15 days of OVX; $p < 0.001$). OVX rats showed the expected decrease in uterus weight and an increase in serum luteinizing hormone (LH) (data not shown), confirming the efficiency of the OVX procedure (Martínez de Morentin et al., 2014, 2015). As expected, central (intracerebroventricular, ICV) E2 treatment elicited a marked decrease in body weight and feeding (Figures 1A and 1B), as well as a reduction in adiposity and lean mass (Figure 1C). As reported before (Cavalcanti-de-Albuquerque et al., 2014), central E2 administration did not affect oxygen consumption (VO_2 72-hr sham vehicle: 121.16 ± 2.76 mL/g lean mass; VO_2 72-hr OVX vehicle: 114.66 ± 3.13 mL/g lean mass; VO_2 72-hr OVX E2: 118.17 ± 3.1 mL/g lean mass). However, central E2 significantly augmented the energy expenditure (EE) of OVX rats (Figure 1D). In keeping with this evidence, OVX rats receiving ICV E2 showed a reduced respiratory quotient (RQ; Figure 1E), which is indicative of higher lipid oxidation, as well as an increase in body temperature and in BAT temperature (Figures S1A and S1B), uncoupling protein 1 (UCP1) BAT expression (Figure S1C) and a reduction in the hepatic lipid content (Figure S1D). The selected dose of E2 was formerly demonstrated to be in the physiological range and not to leak to periphery from the cerebrospinal fluid (Martínez de Morentin et al., 2014, 2015).

Next, we investigated the effect of OVX and central E2 replacement on ceramide content in the mediobasal hypothalamus (MBH). We found that OVX induced a marked elevation of hypothalamic ceramide levels and that E2 ICV restored them to the levels observed in sham-operated rats (Figure 1F). Of note, in association to the rise in ceramide concentration, OVX rats showed increased hypothalamic ER stress in the MBH, as demonstrated by the augmented levels of unfolded protein response (UPR) markers, such as phosphorylated inositol-requiring enzyme (pIRE), phosphorylated PKR-like ER kinase (pPERK), phosphorylated eukaryotic initiation factor 2 alpha (peIF2α), and C/EBP homologous protein (CHOP) (Figure 1G). Again, central E2 administration reversed the increased ER stress by blunting the elevated levels of the UPR markers to the levels of those detected in the sham controls. Particularly, the hypothalamic expression of the chaperone glucose regulated protein 78 kDa (GRP78; also called binding immunoglobulin protein [BiP]; see below) was increased after central treatment with E2, as a cellular mechanism to reduce ER stress (Figure 1G).

Pharmacological Inhibition of Hypothalamic Ceramide Synthesis Recapitulates the Effect of Central E2 on Energy Balance through the SNS

Ceramide-induced lipotoxicity has been reported to promote positive energy balance due to reduced thermogenic capacity (Contreras et al., 2014, 2017). Therefore, we aimed to investigate whether inhibition of ceramide synthesis in the hypothalamus of OVX rats might improve their metabolic phenotype. Chronic ICV administration of the ceramide inhibitor myriocin (Ramírez et al., 2013) to OVX rats decreased body weight and adiposity independent of feeding (Figures 1H–1J). This effect was associated with normalization of ceramide and ER stress markers levels in the MBH (Figures 1K and 1L), increased body temperature (Figure 1M), elevated BAT temperature (Figure 1N) and raised UCP1 protein levels in the BAT (Figure 1O), as well as reduced hepatic lipid levels (Figure S1E) of OVX rats. Given that central ceramides have been reported to induce a marked decrease in the activity of the sympathetic nervous system (SNS) innervating BAT (Contreras et al., 2014), we aimed to investigate whether adrenergic receptor blockade affected the central effect of ICV myriocin on BAT thermogenesis of OVX rats. The effect of central administration of myriocin was reversed (in a feeding-independent manner) by pharmacological blockade of beta 3 adrenergic receptor (β3-AR) with the specific antagonist, SR59230A (López et al., 2010; Martínez de Morentin et al., 2014; Contreras et al., 2014, 2017; Martínez-Sánchez et al., 2017a; Seoane-Collazo et al., 2018) (Figures 2A and 2B). The increase in body weight induced by SR59230A was associated with equivalent reversal of ICV myriocin-induced activation of body temperature (Figure 2C), BAT temperature (Figure 2D), and BAT UCP1 expression (Figure 2E).

Silencing of SPTLC Specifically in the VMH Ameliorates ER Stress and the Metabolic Phenotype of OVX Rats

To further investigate the role of *de novo* ceramide synthesis pathway and to dissect in which hypothalamic nucleus those actions take place, we targeted serine palmitoyltransferase long chain base subunit 1 (SPTLC1). This enzyme catalyzes the

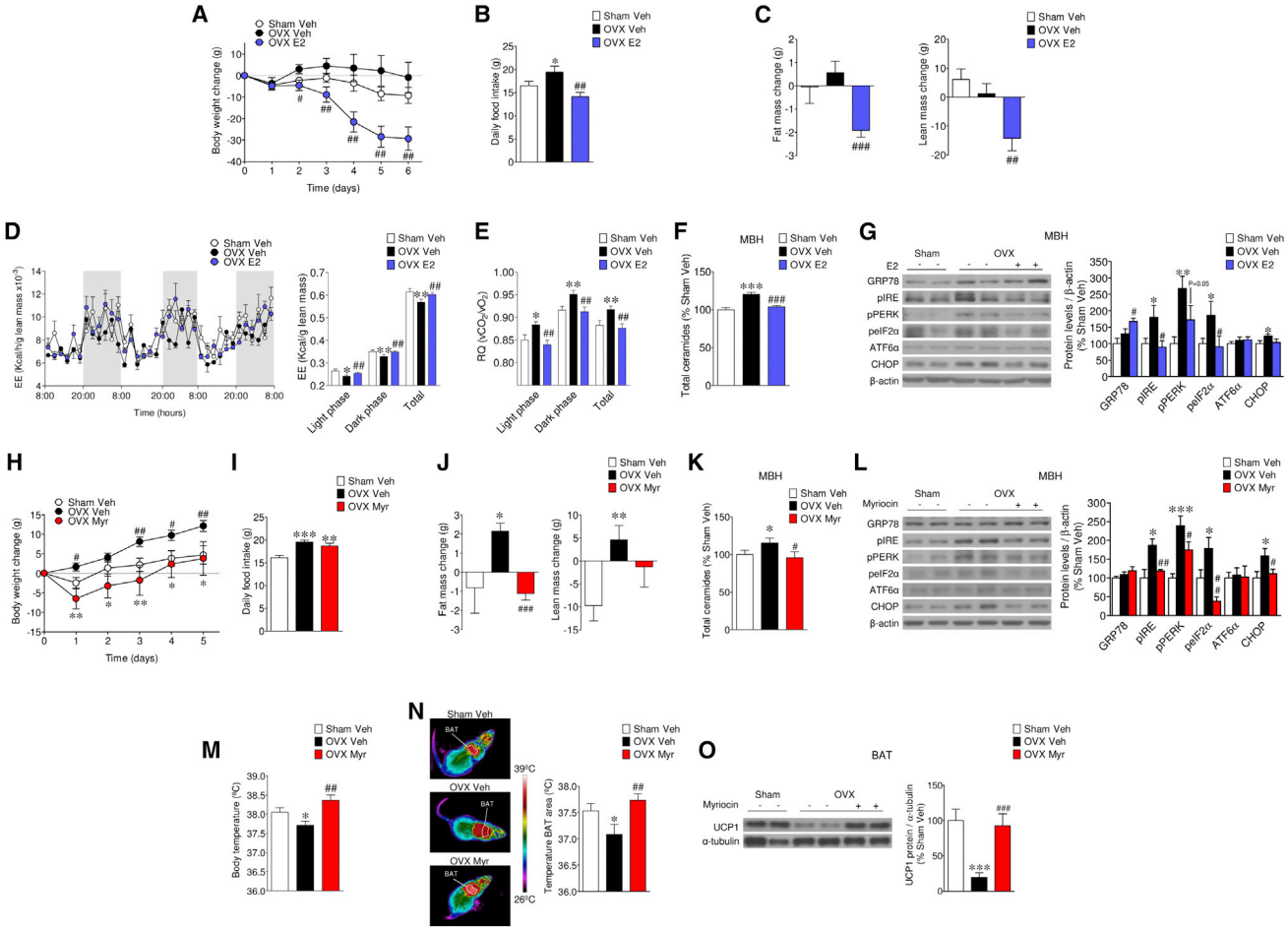

Figure 1. Effect of Central E2 and Myriocin on Energy Balance in OVX Rats

(A–G) Body weight change (A), daily food intake (B), fat mass change (left panel) and lean mass change (right panel) (C), time course energy expenditure (EE) (left panel) and total energy expenditure change (right panel) (D), respiratory quotient (E), ceramide levels in the MBH (F), and representative western blot autoradiographic images (left panel) and MBH protein levels of UPR (right panel) (G) of sham rats or OVX rats ICV treated with vehicle or E2 (n = 7–9 animals per group). (H–O) Body weight change (H), daily food intake (I), fat mass change (left panel) and lean mass change (right panel) (J), ceramide levels in the MBH (K), representative western blot autoradiographic images (left panel) and MBH protein levels of UPR (right panel) (L), body temperature (M), representative infrared thermal images (left panel) and temperature of BAT area (right panel) (N), and representative western blot autoradiographic images (left panel) and protein levels of UCP1 in the BAT (right panel) (O) of sham rats or OVX rats ICV treated with vehicle or myriocin (n = 7–16 animals per group for all the analyses, but the body weight and food intake measurements were n = 28–38).

All data are expressed as mean ± SEM. *, **, and ***p < 0.05, 0.01, and 0.001 versus sham vehicle; #, ##, and ### p < 0.05, 0.01, and 0.001 versus OVX vehicle. For the western blot analyses, representative images for all proteins are shown; in the case of the loading controls a representative gel is displayed for clarity, although each band of each protein was always corrected by its own internal control band (β-actin or α-tubulin). The bands for each picture always come from the same gel, although they have been spliced for clarity.

See also Figure S1.

limiting first step in the *de novo* synthesis of ceramides: the condensation of palmitoyl-CoA and serine, producing 3-ketosphinganine. The SPTLC is composed of two subunits (SPTLC1 and 2); both are essential for enzyme function because they constitute its catalytic core (Hanada, 2003; Yard et al., 2007; Watson et al., 2009). Therefore, we silenced SPTLC1 expression by using adenoviruses harboring a small hairpin RNA (shRNA) or control adenoviruses expressing green fluorescence protein (GFP) alone (Watson et al., 2009), specifically in the VMH, a key hypothalamic nucleus modulating thermogenesis (Morrison et al., 2014; Contreras et al., 2015). Infection in the VMH was assessed by visualization of GFP expression (Figure 3A) and by decreased protein levels of SPTLC1 (Figure 3B). Given that the stability of the SPTLC2 subunit is inherently dependent on the expression of SPTLC1 and both subunits associate with a 1:1 molar stoichiometry (Hanada, 2003; Watson et al., 2009), silencing SPTLC1 also led to an attendant reduction in the expression of SPTLC2 (Figure 3B), as expected and as previously shown (Watson et al., 2009).

Administration of adenoviruses encoding shSPTLC1 in the VMH induced a feeding-independent weight loss in OVX rats, but not in sham rats (Figures 3C–3F). This effect was associated

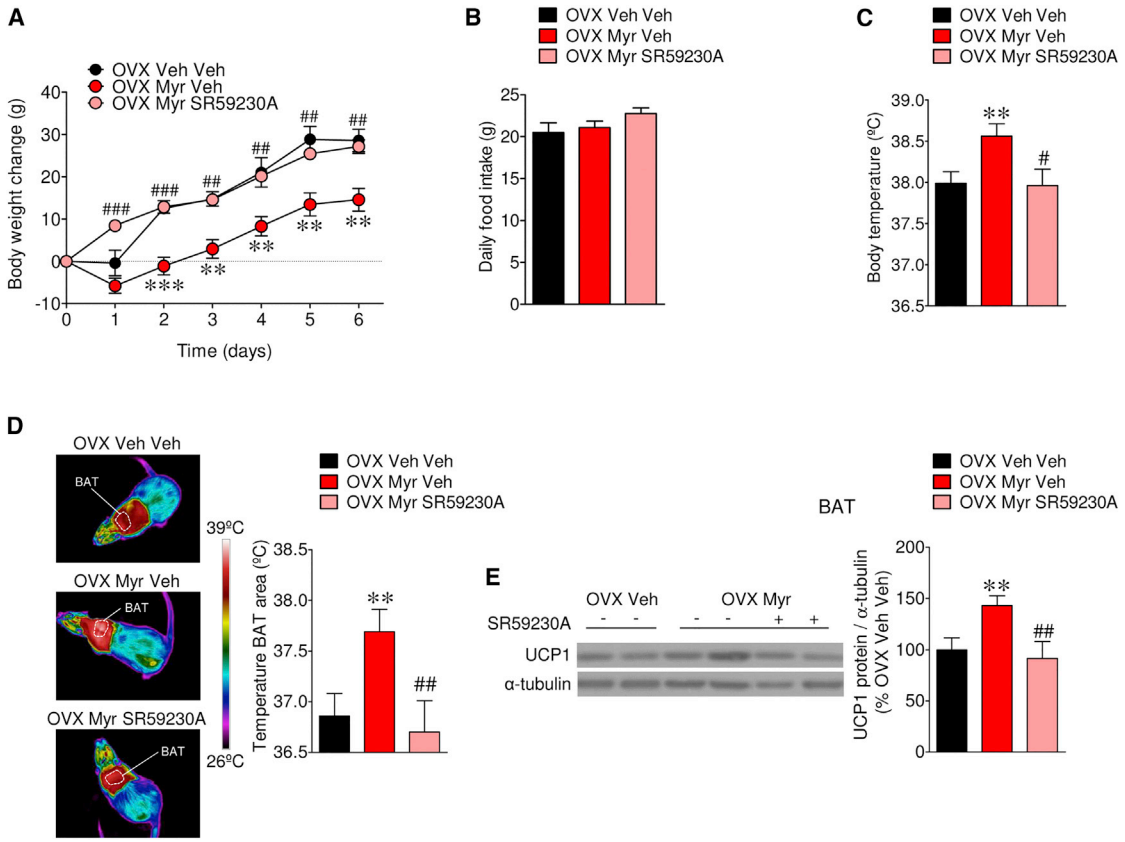

Figure 2. Effect of Myriocin and β3-AR Antagonism on BAT Thermogenesis in OVX Rats

(A–E) Body weight change (A), daily food intake (B), body temperature (C), representative infrared thermal images (left panel) and temperature of BAT area (right panel) (D), and representative western blot autoradiographic images (left panel) and protein levels of UCP1 in the BAT (right panel) (E) of OVX rats ICV treated with myriocin and subcutaneously treated with vehicle or the β3-AR antagonist SR59230A (n = 7–18 animals per group).

All data are expressed as mean ± SEM. ** and ***p < 0.01 and 0.001 versus OVX vehicle vehicle; #, ##, and ### p < 0.05, 0.01, and 0.001 versus OVX myriocin vehicle. For the western blot analyses, representative images for all proteins are shown; in the case of the loading controls a representative gel is displayed for clarity, although each band of each protein was always corrected by its own internal control band (α-tubulin). The bands for each picture always come from the same gel, although they have been spliced for clarity.

with a marked relief of ER stress in the VMH of OVX rats, as demonstrated by the reduced protein levels of pIRE, pPERK, peIF2α, ATF6α, and CHOP, which were also observed in sham rats, but to a lesser extent (Figures 3G–3H). In keeping with these data, injection of shSPTLC1 adenoviruses led to increased body temperature (Figures 4A and 4B), BAT temperature (Figures 4C and 4D) and UCP1 protein levels in the BAT (Figures 4E and 4F) of OVX, but not of sham, rats. These effects were associated with an improvement in the metabolic phenotype of OVX rats, as demonstrated by decreased hepatic steatosis (Figure S2A). Overall, these results, alongside the myriocin data, indicate that the hypothalamic and, more precisely, VMH ceramide levels mediated the central actions of E2 on BAT thermogenesis and energy balance.

Pharmacological Inhibition of Hypothalamic ER Stress Recapitulates the Effect of Central E2 on Energy Balance

Increased hypothalamic ER stress has been associated with the development of insulin and leptin resistance, leading to obesity (Zhang et al., 2008; Ozcan et al., 2009; van Dam et al., 2015; Schneeberger et al., 2013; Contreras et al., 2014, 2017). Bearing in mind that hypothalamic ceramides elicit ER stress (Contreras et al., 2014, 2017), we aimed to investigate whether ceramide-induced ER stress may be a mechanism mediating the central actions of E2 deficiency on BAT thermogenesis and energy homeostasis. Thus, OVX rats were ICV treated with the chemical chaperone tauroursodeoxycholic acid (TUDCA) (Zhang et al., 2008; Ozcan et al., 2009; Schneeberger et al., 2013; Imbernon et al., 2016; Contreras et al., 2017; Porteiro et al., 2017). Central administration of this drug to OVX, but not sham, rats induced feeding-independent weight loss (Figures 5A–5D), decreased hypothalamic ER stress (Figures 5E and 5F), a trend to increase body temperature (Figure 5G), elevated BAT temperature (Figure 5H) and UCP1 protein levels in BAT (Figure 5I). Of note, none of the metabolic changes were found in sham rats (Figures 5G–5I), which is in line with the fact that they did not show elevated ER stress (Figures 1G and 1L). Furthermore, the central injection of TUDCA reduced the hepatic lipid content of OVX rats but had no effects in sham rats (Figure S3A).

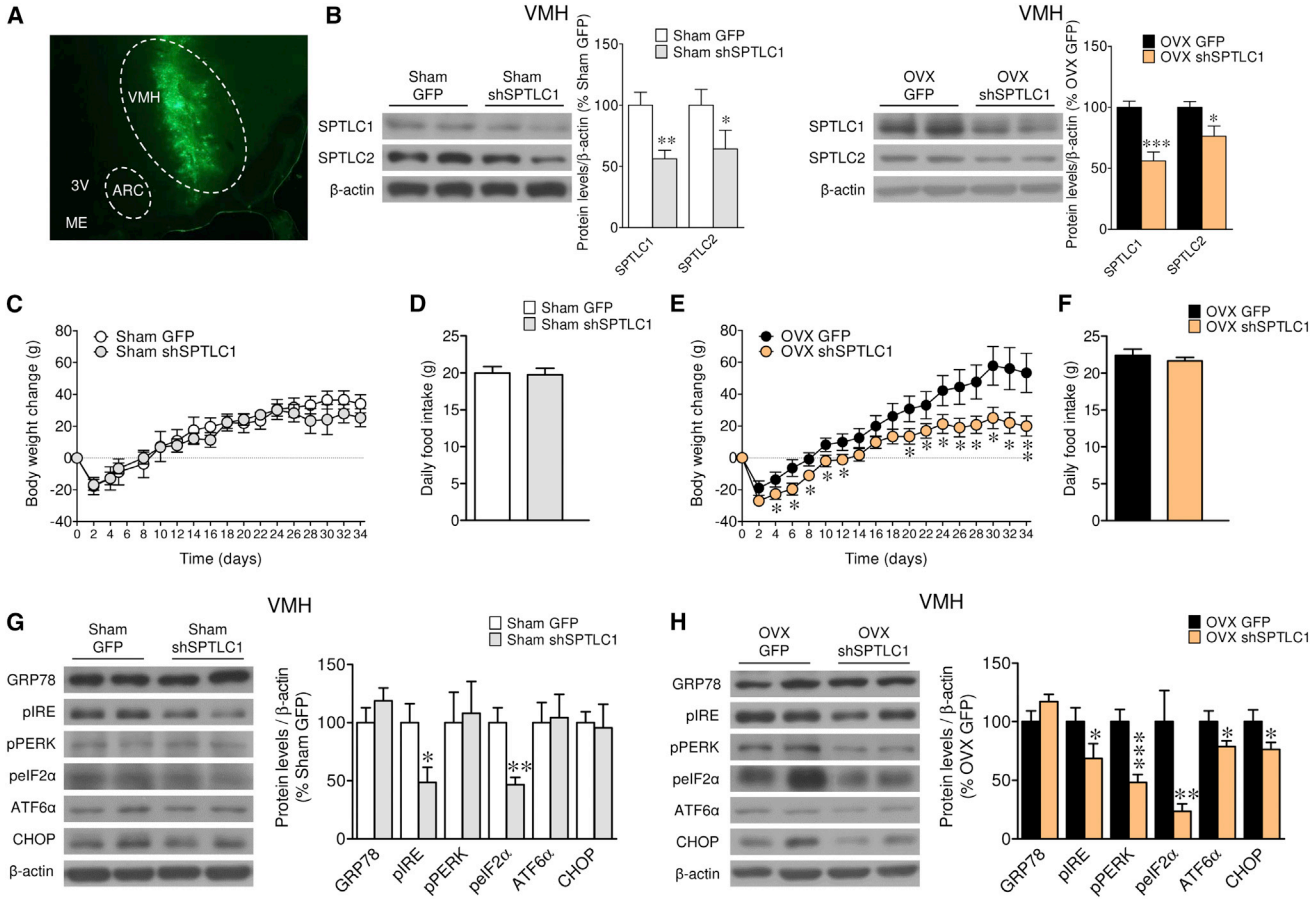

Figure 3. Effect of SPTLC1 Downregulation in the VMH of OVX Rats on Energy Balance

(A–H) Direct fluorescence of GFP (A), representative western blot autoradiographic images (left panel) and VMH protein levels of serine palmitoyltransferase, long chain subunit 1-2 (right panel) (B), body weight change (C and E), daily food intake (D and F), and representative western blot autoradiographic images (left panel) and VMH protein levels of UPR (right panel) (G and H) of sham or OVX rats stereotaxically treated with adenoviruses encoding GFP or shSPTLC1 into the VMH (n = 7–20 animals per group).

All data are expressed as mean ± SEM. *, ** and ***p < 0.05, 0.01, and 0.001 versus sham GFP or OVX GFP. For the western blot analyses, representative images for all proteins are shown; in the case of the loading controls a representative gel is displayed for clarity, although each band of each protein was always corrected by its own internal control band (β-actin). The bands for each picture always come from the same gel, although they have been spliced for clarity.

See also Figure S2.

GRP78 in the VMH Decreases Body Weight and Improves the Metabolic Phenotype of OVX Rats through the SNS

Our first set of data showed that central treatment with E2 decreased ER stress and augmented the hypothalamic protein levels of GRP78 (Figure 1G). This was of importance because this protein is a chaperone, located in the ER, that facilitates the protein folding upstream of the UPR and therefore decreases ER stress levels (Gregor and Hotamisligil, 2011; Fu et al., 2012). Thus, a gain of function experiment was undertaken using an adenovirus encoding GRP78 or control adenoviruses expressing GFP alone injected into the VMH of OVX rats and their sham controls. Infection efficiency in the VMH was assessed by expression of GFP (similarly to Figure 3A; data not shown), and by increased concentration of GRP78 in the VMH (Figures 6E and 6F). GRP78 adenoviruses into the VMH induced feeding-independent weight loss in OVX rats, but not in sham rats (Figures 6A–6D). That effect was linked to decreased ER stress in the VMH of OVX, but not sham, rats (Figures 6E and 6F), increased body temperature (Figure 6G), BAT temperature (Figure 6H), and augmented UCP1 protein levels in BAT (Figure 6I). Notably, central administration of GRP78 in the VMH reduced the hepatic lipid content of OVX rats (Figure S3B).

Finally, we investigated whether regulation of BAT following administration of GRP78 adenoviral particles in the VMH of OVX rats was mediated by the SNS. Pharmacological inactivation of β3-AR by SC administration of the specific antagonist, SR59230A (López et al., 2010; Martínez de Morentin et al., 2014; Contreras et al., 2014, 2017; Martínez-Sánchez et al., 2017a; Seoane-Collazo et al., 2018), prevented the effect on body weight associated with central administration of GRP78 viruses (Figure 7A) without affecting feeding (Figure 7B). Consistently, the treatment with SR59230A blunted the GRP78-induced

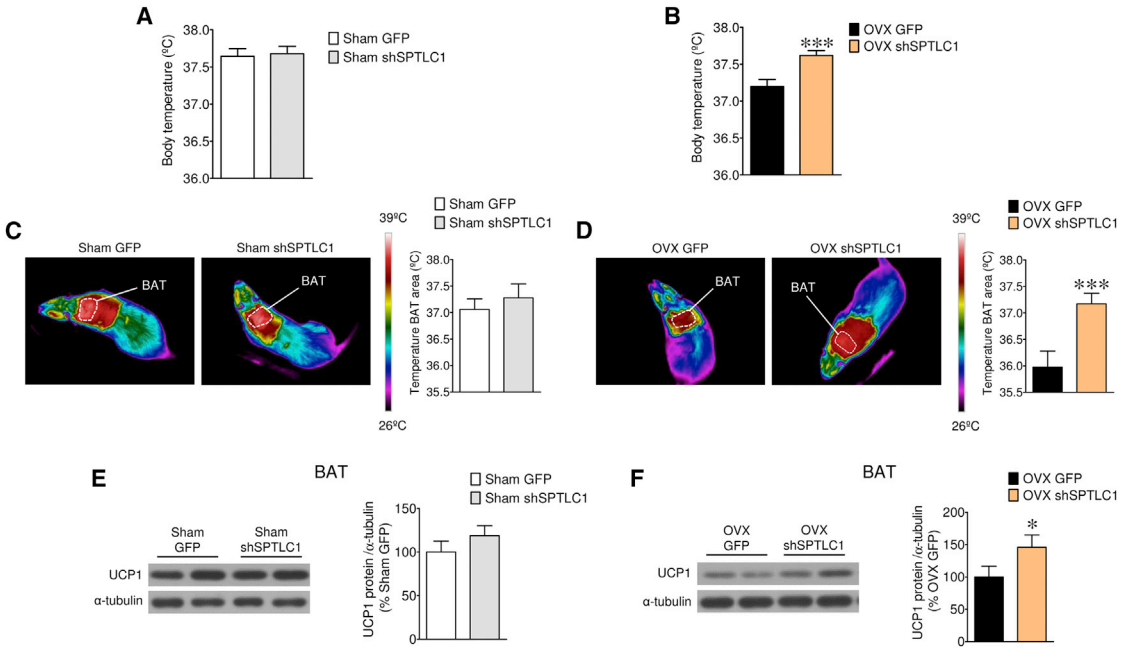

Figure 4. Effect of SPTLC1 Downregulation in the VMH of OVX Rats on BAT Thermogenesis

(A–F) Body temperature (A and B), representative infrared thermal images (left panel) and temperature of BAT area (right panel) (C and D), and representative western blot autoradiographic images (left panel) and protein levels of UCP1 in the BAT (right panel) (E and F) of sham or OVX rats stereotaxically treated in the VMH with adenoviruses encoding GFP or shSPTLC1 (n = 7–20 animals per group).

All data are expressed as mean ± SEM. * and ***$p < 0.05$ and 0.001 versus sham GFP or OVX GFP. For the western blot analyses, representative images for all proteins are shown; in the case of the loading controls a representative gel is displayed for clarity, although each band of each protein was always corrected by its own internal control band (α-tubulin). The bands for each picture always come from the same gel, although they have been spliced for clarity.

See also Figure S2.

increase in body temperature (Figure 7C), BAT temperature (Figure 7D), and UCP1 protein levels in the BAT (Figure 7E). Overall, this evidence demonstrates that E2-induced decrease of ER stress in the VMH is an important modulator of energy balance by controlling BAT thermogenesis.

DISCUSSION

This study identifies a link between the effects of E2 on hypothalamic ceramide-induced lipotoxicity and ER stress with BAT thermogenesis. We demonstrate that central E2 replacement restored hypothalamic ceramide levels and ER stress in OVX female rats. Of note, pharmacological or genetic blockade of ceramide synthesis and relief of ER stress recapitulate the effects of E2, namely increased BAT thermogenesis, weight loss, and reduced hepatic lipids.

Conditions of estrogen deficiency, such as ovariectomy or menopause, are associated with a positive energy balance, as result of hyperphagia and decreased energy expenditure, leading to enhanced adiposity (Mauvais-Jarvis et al., 2013, 2017; Palmer and Clegg, 2015; Mauvais-Jarvis, 2015; Morselli et al., 2016; López and Tena-Sempere, 2017), hepatic lipid accumulation, and steatosis (Paquette et al., 2007; Völzke et al., 2007; Paquette et al., 2008) in animal models and humans. Peripheral and central estrogen replacement therapy reverts this phenotype both in women and in female rodents (Mauvais-Jarvis et al., 2013, 2017; Palmer and Clegg, 2015; Mauvais-Jarvis, 2015; Morselli et al., 2016; López and Tena-Sempere, 2017). Recent evidence indicates that AMP-activated protein kinase (AMPK) in the VMH mediates the central effect of E2 on BAT thermogenesis through the SNS (Martínez de Morentin et al., 2014, 2015). Considering the key role of AMPK on fatty acid metabolism (Kahn et al., 2005; Lage et al., 2008; López et al., 2016), this evidence directly links the central effects of estrogens with hypothalamic lipids. However, despite recent data showing sexual dimorphism in brain fatty acid content (Rodriguez-Navas et al., 2016) and even though peripheral E2 treatment reduces serum ceramide levels in OVX rats (Vinayavekhin et al., 2016), whether complex lipids metabolism is involved in the central actions of E2 remains unclear. This is relevant, because the hormonal regulation of lipid metabolism usually shows tissue-specific effects (López et al., 2010; Martínez-Sánchez et al., 2017a). In this sense, we have recently reported that thyroid hormones (THs) modulate ceramide metabolism in an opposite fashion within different brain areas, such as the hypothalamus and the cerebral cortex (Martínez-Sánchez et al., 2017a). Therefore, the fact that systemic E2 decreased serum ceramide levels (Vinayavekhin et al., 2016) did not imply a similar hypothalamic effect.

Compelling evidence indicates that hypothalamic ceramide-induced lipotoxicity is a pathological mechanism leading to obesity by suppressing BAT thermogenesis (Contreras et al., 2014, 2017). Importantly, pharmacological or genetic targeting

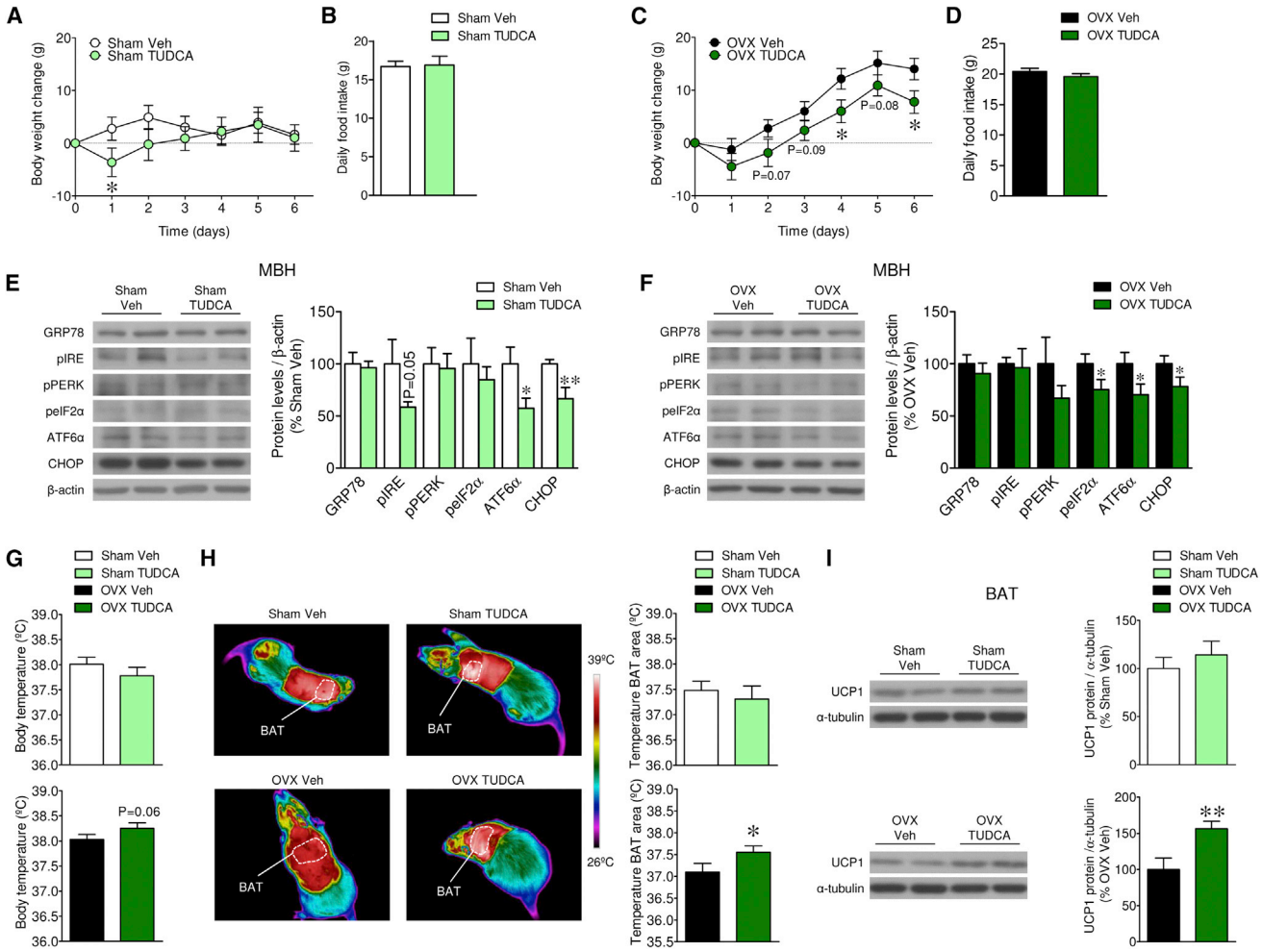

Figure 5. Effect of Central TUDCA on Energy Balance in OVX Rats

(A–I) Body weight change (A and C), daily food intake (B and D), representative western blot autoradiographic images (left panel) and MBH protein levels of UPR (right panel) (E and F), body temperature (G), representative infrared thermal images (left panel) and temperature of BAT area (right panel) (H), and representative western blot autoradiographic images (left panel) and protein levels of UCP1 in the BAT (right panel) (I) of sham or OVX rats ICV treated with vehicle or TUDCA (n = 7–8 animals per group).

All data are expressed as mean ± SEM.* and **p < 0.05 and 0.01 versus sham vehicle or OVX vehicle. For the western blot analyses, representative images for all proteins are shown; in the case of the loading controls a representative gel is displayed for clarity, although each band of each protein was always corrected by its own internal control band (β-actin or α-tubulin). The bands for each picture always from come from the same gel, although they have been spliced for clarity. See also Figure S3.

of this pathway, causing reduced ceramide concentration and/or decreased ER stress ameliorates obesity (Contreras et al., 2014, 2017). However, it remains totally unknown whether fluctuations in ceramide levels and/or ER stress reflect brain changes associated with, for example, neuronal and/or glial metabolic activity (Picard et al., 2013, 2014; Magnan et al., 2015), or whether they might respond to or integrate nutritional and hormonal cues from the periphery (López et al., 2016). Supporting this latter idea, several endocrine signals, such as THs (López et al., 2010; Alvarez-Crespo et al., 2016; Martínez-Sánchez et al., 2017a, b), leptin (Wolfgang et al., 2007; Tanida et al., 2013), bone-morphogenetic protein 8B (BMP8B) (Whittle et al., 2012; Martins et al., 2016), glucagon-like peptide 1 (GLP-1) (Beiroa et al., 2014), and, importantly, E2 (Martínez de Morentin et al., 2014, 2015), have been shown to regulate hypothalamic fatty acid metabolism to modulate energy balance.

Thus, we hypothesized that E2-induced actions on energy balance could be mediated by modulation of hypothalamic ceramides and ER stress. Our data showed that central treatment with E2 induced a negative energy balance in OVX rats, associated with a reduction of hypothalamic ceramide-induced lipotoxicity and ER stress. Of note, central pharmacological inhibition of ceramide synthesis by using the SPTLC inhibitor myriocin suppressed hypothalamic ER stress and fully recapitulated the effects of E2 on energy balance. Next, we aimed to further investigate the specific hypothalamic nuclei where those actions take place. It is known that the VMH plays a major role in the modulation of BAT thermogenesis (Morrison et al., 2014;

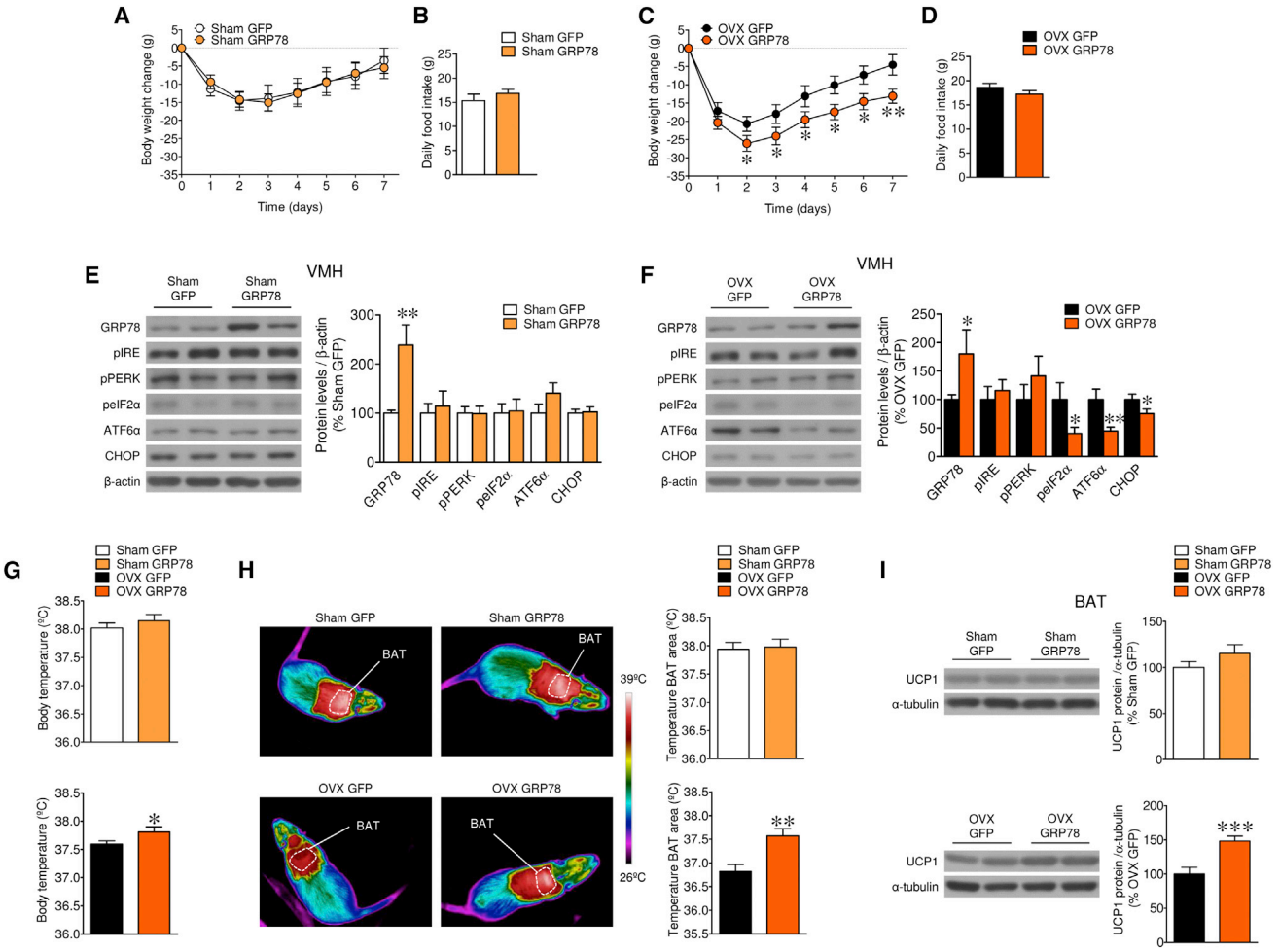

Figure 6. Effect of GRP78 Overexpression in the VMH of OVX Rats on Energy Balance and BAT Thermogenesis

(A–I) Body weight change (A and C), daily food intake (B and D), representative western blot autoradiographic images (left panel) and VMH protein levels of UPR (right panel) (E and F), body temperature (G), representative infrared thermal images (left panel) and temperature of BAT area (right panel) (H), and representative western blot autoradiographic images (left panel) and protein levels of UCP1 in the BAT (right panel) (I) of sham or OVX rats stereotaxically treated in the VMH with adenoviruses encoding GFP or GRP78 (n = 7–18 animals per group).

All data are expressed as mean ± SEM. *, **, and ***$p < 0.05$, 0.01, and 0.001 versus sham GFP or OVX GFP. For the western blot analyses, representative images for all proteins are shown; in the case of the loading controls a representative gel is displayed for clarity, although each band of each protein was always corrected by its own internal control band (β-actin or α-tubulin). The bands for each picture always come from the same gel, although they have been spliced for clarity. See also Figure S3.

Contreras et al., 2015) and that ERα is the site of action for E2 in the VMH to drive the modulation of BAT thermogenic function (Musatov et al., 2007; Xu et al., 2011; Martínez de Morentin et al., 2014, 2015). Therefore, following a genetic strategy we silenced SPTLC1 expression in the VMH of OVX obese rats. Specific downregulation of SPTLC exclusively in the VMH ameliorated ER stress and obesity and improved the metabolic health of OVX rats, including a reduction in hepatic lipid content. Overall, these data suggest that central E2 induces a negative energy balance by diminishing ceramide-induced lipotoxicity and ER stress, a hypothesis that was proven by treating OVX rats centrally with the chemical chaperone TUDCA or by genetically overexpressing the chaperone GRP78 within the VMH. Importantly, all the above effects were reversed by pharmacological blockage of β3-AR, therefore suggesting that VMH changes in ceramide signaling and hypothalamic ER stress induced by E2 to increase thermogenesis are conveyed via the sympathetic outflow to BAT.

In summary, in this study we demonstrate that E2 promotes an amelioration of ceramide-induced lipotoxicity and ER stress, specifically in the VMH. This action leads to increased BAT thermogenesis through the activation of sympathetic β3-AR signaling, an action that is associated with feeding-independent weight loss and reduced hepatic steatosis, as well as with a substantial attenuation (or reversal) of some of the metabolic hallmarks of OVX and menopause, namely, body weight gain, and hepatic steatosis. This evidence is of relevance because proper understanding of gender differences in the

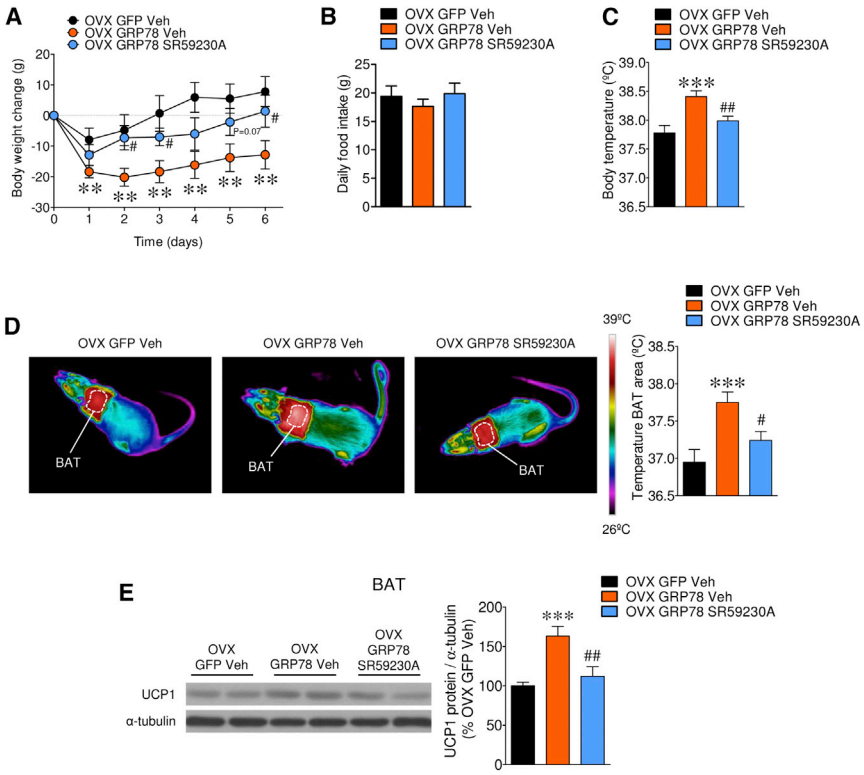

Figure 7. Effect of β3-AR Antagonism on GRP78-Induced BAT Thermogenesis in OVX Rats

(A–E) Body weight change (A), daily food intake (B), body temperature (C), representative infrared thermal images (left panel) and temperature of BAT area (right panel) (D), and representative western blot autoradiographic images (left panel) and protein levels of UCP1 in the BAT (right panel) (E) of OVX rats stereotaxically treated in the VMH with adenoviruses encoding GFP or GRP78 and subcutaneously treated with vehicle or the β_3 adrenoceptor antagonist SR59230A (n = 7–19 animals per group).

All data are expressed as mean ± SEM. ** and ***p < 0.01 and 0.001 versus OVX GFP vehicle; # and ## p < 0.05 and 0.01 versus OVX GRP78 vehicle. For the western blot analyses, representative images for all proteins are shown; in the case of the loading controls a representative gel is displayed for clarity, although each band of each protein was always corrected by its own internal control band (α-tubulin). The bands for each picture always come from the same gel, although they have been spliced for clarity.

regulation of energy balance and how their impairment may lead to obesity have capital importance in the identification (and design) of targets for drug development (Mauvais-Jarvis et al., 2013, 2017; Palmer and Clegg, 2015; Mauvais-Jarvis, 2015; Morselli et al., 2016; López and Tena-Sempere, 2017). In this context, our data provide insights into the physiological regulation of energy balance and its perturbation in estrogen-deficient states and suggest that the ceramide metabolism and ER stress may be a potential therapeutic target for the treatment of obesity associated with conditions of estrogen deficiency.

STAR★METHODS

Detailed methods are provided in the online version of this paper and include the following:

- KEY RESOURCES TABLE
- CONTACT FOR REAGENT AND RESOURCE SHARING
- EXPERIMENTAL MODEL AND SUBJECT DETAILS
  - Animals and housing conditions
- METHOD DETAILS
  - Ovariectomy
  - Central and peripheral treatments
  - Stereotaxic microinjection of adenoviral vectors
  - Temperature measurements
  - Calorimetric system and nuclear magnetic resonance
  - Sample processing
  - Ceramide quantification
  - Histological analyses
  - Western blotting
- QUANTIFICATION AND STATISTICAL ANALYSIS

SUPPLEMENTAL INFORMATION

Supplemental Information includes three figures and can be found with this article online at https://doi.org/10.1016/j.celrep.2018.09.038.

ACKNOWLEDGMENTS

We dedicate this work to the bright memory of our colleague, master, and friend Enrique Aguilar. The research leading to these results received funding from the European Community's Seventh Framework Programme (FP7/2007-2013) for the ObERStress European Research Council Project (281854 to M.L.), Xunta de Galicia (EM 2012/039 and 2012-CP069 to R.N.; 2015-CP079 to M.L.), Junta de Andalucía (P12-FQM-01943 to M.T.-S.), MINECO, which was co-funded by the FEDER Program of EU (BFU2011-29102 to C.D.; BFU2012-35255 to R.N.; BFU2014-57581-P to M.T.-S.; SAF2015-71026-R and BFU2015-70454-REDT/Adipoplast to M.L.), and the Stiftelsen Kristian Gerhard Jebsen and Western Norway Regional Health Authority (to J.F.). I.G.-G. received a fellowship from MINECO (FPU12/01827); C.C. received a Sara Borrell Contract from ISCIII (CD14/0007); A.E.-S. received a fellowship from MINECO (FPI/BES-2016-077439); L.L.-P. received a fellowship from Xunta de Galicia (ED481A-2016/094); and E.R.-P. received a fellowship from MINECO (FPI/BES-2015-072743). The CiMUS is supported by the Xunta de Galicia (2016-2019, ED431G/05). CIBER de Fisiopatología de la Obesidad y Nutrición is an initiative of ISCIII. The funders had no role in study design, data collection and analysis, decision to publish, or preparation of the manuscript.

AUTHOR CONTRIBUTIONS

I.G.-G., C.C., Á.E.-S., I.P., L.L.-P., E.R.-P., P.B.M.d.M., and F.R.-P. performed the *in vivo* experiments (ovariectomy; peripheral, central, and stereotaxic microinjections; temperature measurements; calorimetric system; and nuclear magnetic resonance) and the analytical methods (temperature and hormone measurements; histological analyses; and western blotting) and collected and analyzed the data. H.L., B.C., and C.M. performed the ceramide analysis, which were also developed in facilities of the Institute of Advanced Chemistry of Catalonia (Spain). I.G.-G., J.F., C.D., R.N., H.L., C.M., M.T.-S., and M.L. analyzed, discussed, and interpreted the data. I.G.-G. and M.L. designed the experiments, wrote the manuscript, and made the figures. All authors reviewed and edited the manuscript and had final approval of the submitted version. M.L. developed the hypothesis; coordinated and directed the project; and secured funding.

DECLARATION OF INTERESTS

The authors declare no competing interests.

Received: May 22, 2017
Revised: August 22, 2018
Accepted: September 11, 2018
Published: October 9, 2018

REFERENCES

Alvarez-Crespo, M., Csikasz, R.I., Martínez-Sánchez, N., Diéguez, C., Cannon, B., Nedergaard, J., and López, M. (2016). Essential role of UCP1 modulating the central effects of thyroid hormones on energy balance. Mol. Metab. *5*, 271–282.

Beiroa, D., Imbernon, M., Gallego, R., Senra, A., Herranz, D., Villarroya, F., Serrano, M., Fernø, J., Salvador, J., Escalada, J., et al. (2014). GLP-1 agonism stimulates brown adipose tissue thermogenesis and browning through hypothalamic AMPK. Diabetes *63*, 3346–3358.

Cavalcanti-de-Albuquerque, J.P., Salvador, I.C., Martins, E.L., Jardim-Messeder, D., Werneck-de-Castro, J.P., Galina, A., and Carvalho, D.P. (2014). Role of estrogen on skeletal muscle mitochondrial function in ovariectomized rats: a time course study in different fiber types. J. Appl. Physiol (1985) *116*, 779–789.

Contreras, C., González-García, I., Martínez-Sánchez, N., Seoane-Collazo, P., Jacas, J., Morgan, D.A., Serra, D., Gallego, R., González, F., Casals, N., et al. (2014). Central ceramide-induced hypothalamic lipotoxicity and ER stress regulate energy balance. Cell Rep. *9*, 366–377.

Contreras, C., González, F., Fernø, J., Diéguez, C., Rahmouni, K., Nogueiras, R., and López, M. (2015). The brain and brown fat. Ann. Med. *47*, 150–168.

Contreras, C., Gonzalez-Garcia, I., Seoane-Collazo, P., Martínez-Sánchez, N., Linares-Pose, L., Rial-Pensado, E., Ferno, J., Tena-Sempere, M., Casals, N., Dieguez, C., et al. (2017). Reduction of hypothalamic endoplasmic reticulum stress activates browning of white fat and ameliorates obesity. Diabetes *66*, 87–99.

Cui, H., López, M., and Rahmouni, K. (2017). The cellular and molecular bases of leptin and ghrelin resistance in obesity. Nat. Rev. Endocrinol. *13*, 338–351.

Folch, J., Lees, M., and Sloane Stanley, G.H. (1957). A simple method for the isolation and purification of total lipides from animal tissues. J. Biol. Chem. *226*, 497–509.

Fu, S., Watkins, S.M., and Hotamisligil, G.S. (2012). The role of endoplasmic reticulum in hepatic lipid homeostasis and stress signaling. Cell Metab. *15*, 623–634.

Gregor, M.F., and Hotamisligil, G.S. (2011). Inflammatory mechanisms in obesity. Annu. Rev. Immunol. *29*, 415–445.

Hanada, K. (2003). Serine palmitoyltransferase, a key enzyme of sphingolipid metabolism. Biochim. Biophys. Acta *1632*, 16–30.

Imbernon, M., Beiroa, D., Vázquez, M.J., Morgan, D.A., Veyrat-Durebex, C., Porteiro, B., Díaz-Arteaga, A., Senra, A., Busquets, S., Velásquez, D.A., et al. (2013). Central melanin-concentrating hormone influences liver and adipose metabolism via specific hypothalamic nuclei and efferent autonomic/JNK1 pathways. Gastroenterology *144*, 636–649.e6.

Imbernon, M., Sanchez-Rebordelo, E., Romero-Picó, A., Kalló, I., Chee, M.J., Porteiro, B., Al-Massadi, O., Contreras, C., Fernø, J., Senra, A., et al. (2016). Hypothalamic kappa opioid receptor mediates both diet-induced and melanin concentrating hormone-induced liver damage through inflammation and endoplasmic reticulum stress. Hepatology *64*, 1086–1104.

Kahn, B.B., Alquier, T., Carling, D., and Hardie, D.G. (2005). AMP-activated protein kinase: ancient energy gauge provides clues to modern understanding of metabolism. Cell Metab. *1*, 15–25.

Lage, R., Diéguez, C., Vidal-Puig, A., and López, M. (2008). AMPK: a metabolic gauge regulating whole-body energy homeostasis. Trends Mol. Med. *14*, 539–549.

López, M., and Tena-Sempere, M. (2015). Estrogens and the control of energy homeostasis: a brain perspective. Trends Endocrinol. Metab. *26*, 411–421.

López, M., and Tena-Sempere, M. (2017). Estradiol effects on hypothalamic AMPK and BAT thermogenesis: A gateway for obesity treatment? Pharmacol. Ther. *178*, 109–122.

López, M., Lage, R., Saha, A.K., Pérez-Tilve, D., Vázquez, M.J., Varela, L., Sangiao-Alvarellos, S., Tovar, S., Raghay, K., Rodríguez-Cuenca, S., et al. (2008). Hypothalamic fatty acid metabolism mediates the orexigenic action of ghrelin. Cell Metab. *7*, 389–399.

López, M., Varela, L., Vázquez, M.J., Rodríguez-Cuenca, S., González, C.R., Velagapudi, V.R., Morgan, D.A., Schoenmakers, E., Agassandian, K., Lage, R., et al. (2010). Hypothalamic AMPK and fatty acid metabolism mediate thyroid regulation of energy balance. Nat. Med. *16*, 1001–1008.

López, M., Nogueiras, R., Tena-Sempere, M., and Diéguez, C. (2016). Hypothalamic AMPK: a canonical regulator of whole-body energy balance. Nat. Rev. Endocrinol. *12*, 421–432.

Magnan, C., Levin, B.E., and Luquet, S. (2015). Brain lipid sensing and the neural control of energy balance. Mol. Cell. Endocrinol. *418*, 3–8.

Martínez de Morentin, P.B., and López, M. (2010). "Mens sana in corpore sano": exercise and hypothalamic ER stress. PLoS Biol. *8*, e1000464.

Martínez de Morentin, P.B., Whittle, A.J., Fernø, J., Nogueiras, R., Diéguez, C., Vidal-Puig, A., and López, M. (2012). Nicotine induces negative energy balance through hypothalamic AMP-activated protein kinase. Diabetes *61*, 807–817.

Martínez de Morentin, P.B., González-García, I., Martins, L., Lage, R., Fernández-Mallo, D., Martínez-Sánchez, N., Ruíz-Pino, F., Liu, J., Morgan, D.A., Pinilla, L., et al. (2014). Estradiol regulates brown adipose tissue thermogenesis via hypothalamic AMPK. Cell Metab. *20*, 41–53.

Martínez de Morentin, P.B., Lage, R., González-García, I., Ruíz-Pino, F., Martins, L., Fernández-Mallo, D., Gallego, R., Fernø, J., Señarís, R., Saha, A.K., et al. (2015). Pregnancy induces resistance to the anorectic effect of hypothalamic malonyl-CoA and the thermogenic effect of hypothalamic AMPK inhibition in female rats. Endocrinology *156*, 947–960.

Martínez-Sánchez, N., Seoane-Collazo, P., Contreras, C., Varela, L., Villarroya, J., Rial-Pensado, E., Buqué, X., Aurrekoetxea, I., Delgado, T.C., Vázquez-Martínez, R., et al. (2017a). Hypothalamic AMPK-ER stress-JNK1 axis mediates the central actions of thyroid hormones on energy balance. Cell Metab. *26*, 212–229.e12.

Martínez-Sánchez, N., Moreno-Navarrete, J.M., Contreras, C., Rial-Pensado, E., Fernø, J., Nogueiras, R., Diéguez, C., Fernández-Real, J.M., and López, M. (2017b). Thyroid hormones induce browning of white fat. J. Endocrinol. *232*, 351–362.

Martins, L., Seoane-Collazo, P., Contreras, C., González-García, I., Martínez-Sánchez, N., González, F., Zalvide, J., Gallego, R., Diéguez, C., Nogueiras, R., et al. (2016). A functional link between AMPK and orexin mediates the effect of BMP8B on energy balance. Cell Rep. *16*, 2231–2242.

Mauvais-Jarvis, F. (2015). Sex differences in metabolic homeostasis, diabetes, and obesity. Biol. Sex Differ. *6*, 14.

Mauvais-Jarvis, F., Clegg, D.J., and Hevener, A.L. (2013). The role of estrogens in control of energy balance and glucose homeostasis. Endocr. Rev. *34*, 309–338.

Mauvais-Jarvis, F., Arnold, A.P., and Reue, K. (2017). A guide for the design of pre-clinical studies on sex differences in metabolism. Cell Metab. *25*, 1216–1230.

Merchenthaler, I., Lane, M.V., Numan, S., and Dellovade, T.L. (2004). Distribution of estrogen receptor alpha and beta in the mouse central nervous system: in vivo autoradiographic and immunocytochemical analyses. J. Comp. Neurol. *473*, 270–291.

Morrison, S.F., Madden, C.J., and Tupone, D. (2014). Central neural regulation of brown adipose tissue thermogenesis and energy expenditure. Cell Metab. *19*, 741–756.

Morselli, E., Frank, A.P., Santos, R.S., Fátima, L.A., Palmer, B.F., and Clegg, D.J. (2016). Sex and gender: critical variables in pre-clinical and clinical medical research. Cell Metab. *24*, 203–209.

Musatov, S., Chen, W., Pfaff, D.W., Mobbs, C.V., Yang, X.J., Clegg, D.J., Kaplitt, M.G., and Ogawa, S. (2007). Silencing of estrogen receptor alpha in the ventromedial nucleus of hypothalamus leads to metabolic syndrome. Proc. Natl. Acad. Sci. USA *104*, 2501–2506.

Osterlund, M., Kuiper, G.G., Gustafsson, J.A., and Hurd, Y.L. (1998). Differential distribution and regulation of estrogen receptor-alpha and -beta mRNA within the female rat brain. Brain Res. Mol. Brain Res. *54*, 175–180.

Ozcan, L., Ergin, A.S., Lu, A., Chung, J., Sarkar, S., Nie, D., Myers, M.G., Jr., and Ozcan, U. (2009). Endoplasmic reticulum stress plays a central role in development of leptin resistance. Cell Metab. *9*, 35–51.

Palmer, B.F., and Clegg, D.J. (2015). The sexual dimorphism of obesity. Mol. Cell. Endocrinol. *402*, 113–119.

Paquette, A., Shinoda, M., Rabasa Lhoret, R., Prud'homme, D., and Lavoie, J.M. (2007). Time course of liver lipid infiltration in ovariectomized rats: impact of a high-fat diet. Maturitas *58*, 182–190.

Paquette, A., Wang, D., Jankowski, M., Gutkowska, J., and Lavoie, J.M. (2008). Effects of ovariectomy on PPAR alpha, SREBP-1c, and SCD-1 gene expression in the rat liver. Menopause *15*, 1169–1175.

Picard, A., Rouch, C., Kassis, N., Moullé, V.S., Croizier, S., Denis, R.G., Castel, J., Coant, N., Davis, K., Clegg, D.J., et al. (2013). Hippocampal lipoprotein lipase regulates energy balance in rodents. Mol. Metab. *3*, 167–176.

Picard, A., Moullé, V.S., Le Foll, C., Cansell, C., Véret, J., Coant, N., Le Stunff, H., Migrenne, S., Luquet, S., Cruciani-Guglielmacci, C., et al. (2014). Physiological and pathophysiological implications of lipid sensing in the brain. Diabetes Obes. Metab. *16* (*Suppl 1*), 49–55.

Porteiro, B., Fondevila, M.F., Delgado, T.C., Iglesias, C., Imbernon, M., Iruzubieta, P., Crespo, J., Zabala-Letona, A., Fernø, J., González-Terán, B., et al. (2017). Hepatic p63 regulates steatosis via IKKβ/ER stress. Nat. Commun. *8*, 15111.

Ramírez, S., Martíns, L., Jacas, J., Carrasco, P., Pozo, M., Clotet, J., Serra, D., Hegardt, F.G., Diéguez, C., López, M., and Casals, N. (2013). Hypothalamic ceramide levels regulated by CPT1C mediate the orexigenic effect of ghrelin. Diabetes *62*, 2329–2337.

Rodriguez-Navas, C., Morselli, E., and Clegg, D.J. (2016). Sexually dimorphic brain fatty acid composition in low and high fat diet-fed mice. Mol. Metab. *5*, 680–689.

Schneeberger, M., Dietrich, M.O., Sebastián, D., Imbernón, M., Castaño, C., Garcia, A., Esteban, Y., Gonzalez-Franquesa, A., Rodríguez, I.C., Bortolozzi, A., et al. (2013). Mitofusin 2 in POMC neurons connects ER stress with leptin resistance and energy imbalance. Cell *155*, 172–187.

Schneeberger, M., Gomis, R., and Claret, M. (2014). Hypothalamic and brainstem neuronal circuits controlling homeostatic energy balance. J. Endocrinol. *220*, T25–T46.

Scott, M.M., Xu, Y., Elias, C.F., and Williams, K.W. (2014). Central regulation of food intake, body weight, energy expenditure, and glucose homeostasis. Front. Neurosci. *8*, 384.

Seoane-Collazo, P., Martínez de Morentin, P.B., Fernø, J., Diéguez, C., Nogueiras, R., and López, M. (2014). Nicotine improves obesity and hepatic steatosis and ER stress in diet-induced obese male rats. Endocrinology *155*, 1679–1689.

Seoane-Collazo, P., Roa, J., Rial-Pensado, E., Liñares-Pose, L., Beiroa, D., Ruíz-Pino, F., López-González, T., Morgan, D.A., Pardavila, J.A., Sánchez-Tapia, M.J., et al. (2018). SF1-specific AMPKα1 deletion protects against diet-induced obesity. Diabetes, Published August 13, 2018. https://doi.org/10.2337/db17-1538.

Seyer, A., Boudah, S., Broudin, S., Junot, C., and Colsch, B. (2016). Annotation of the human cerebrospinal fluid lipidome using high resolution mass spectrometry and a dedicated data processing workflow. Metabolomics *12*, 91.

Simerly, R.B., Chang, C., Muramatsu, M., and Swanson, L.W. (1990). Distribution of androgen and estrogen receptor mRNA-containing cells in the rat brain: an in situ hybridization study. J. Comp. Neurol. *294*, 76–95.

Simonian, S.X., and Herbison, A.E. (1997). Differential expression of estrogen receptor alpha and beta immunoreactivity by oxytocin neurons of rat paraventricular nucleus. J. Neuroendocrinol. *9*, 803–806.

Tanida, M., Yamamoto, N., Shibamoto, T., and Rahmouni, K. (2013). Involvement of hypothalamic AMP-activated protein kinase in leptin-induced sympathetic nerve activation. PLoS ONE *8*, e56660.

Turpin, S.M., Nicholls, H.T., Willmes, D.M., Mourier, A., Brodesser, S., Wunderlich, C.M., Mauer, J., Xu, E., Hammerschmidt, P., Brönneke, H.S., et al. (2014). Obesity-induced CerS6-dependent C16:0 ceramide production promotes weight gain and glucose intolerance. Cell Metab. *20*, 678–686.

van Dam, A.D., Kooijman, S., Schilperoort, M., Rensen, P.C., and Boon, M.R. (2015). Regulation of brown fat by AMP-activated protein kinase. Trends Mol. Med. *21*, 571–579.

Varela, L., Martínez-Sánchez, N., Gallego, R., Vásquez, M.J., Roa, J., Gándara, M., Schoenmakers, E., Nogueiras, R., Chatterjee, K., Tena-Sempere, M., et al. (2012). Hypothalamic mTOR pathway mediates thyroid hormone-induced hyperphagia in hyperthyroidism. J. Pathol *227*, 209–222.

Vinayavekhin, N., Sueajai, J., Chaihad, N., Panrak, R., Chokchaisiri, R., Sangvanich, P., Suksamrarn, A., and Piyachaturawat, P. (2016). Serum lipidomics analysis of ovariectomized rats under Curcuma comosa treatment. J. Ethnopharmacol. *192*, 273–282.

Voisin, D.L., Simonian, S.X., and Herbison, A.E. (1997). Identification of estrogen receptor-containing neurons projecting to the rat supraoptic nucleus. Neuroscience *78*, 215–228.

Völzke, H., Schwarz, S., Baumeister, S.E., Wallaschofski, H., Schwahn, C., Grabe, H.J., Kohlmann, T., John, U., and Dören, M. (2007). Menopausal status and hepatic steatosis in a general female population. Gut *56*, 594–595.

Watson, M.L., Coghlan, M., and Hundal, H.S. (2009). Modulating serine palmitoyl transferase (SPT) expression and activity unveils a crucial role in lipid-induced insulin resistance in rat skeletal muscle cells. Biochem. J. *417*, 791–801.

Whittle, A.J., Carobbio, S., Martíns, L., Slawik, M., Hondares, E., Vázquez, M.J., Morgan, D., Csikasz, R.I., Gallego, R., Rodriguez-Cuenca, S., et al. (2012). BMP8B increases brown adipose tissue thermogenesis through both central and peripheral actions. Cell *149*, 871–885.

Wolfgang, M.J., Cha, S.H., Sidhaye, A., Chohnan, S., Cline, G., Shulman, G.I., and Lane, M.D. (2007). Regulation of hypothalamic malonyl-CoA by central glucose and leptin. Proc. Natl. Acad. Sci. USA *104*, 19285–19290.

Xu, Y., Nedungadi, T.P., Zhu, L., Sobhani, N., Irani, B.G., Davis, K.E., Zhang, X., Zou, F., Gent, L.M., Hahner, L.D., et al. (2011). Distinct hypothalamic neurons mediate estrogenic effects on energy homeostasis and reproduction. Cell Metab. *14*, 453–465.

Yard, B.A., Carter, L.G., Johnson, K.A., Overton, I.M., Dorward, M., Liu, H., McMahon, S.A., Oke, M., Puech, D., Barton, G.J., et al. (2007). The structure of serine palmitoyltransferase; gateway to sphingolipid biosynthesis. J. Mol. Biol. *370*, 870–886.

Zhang, X., Zhang, G., Zhang, H., Karin, M., Bai, H., and Cai, D. (2008). Hypothalamic IKKbeta/NF-kappaB and ER stress link overnutrition to energy imbalance and obesity. Cell *135*, 61–73.

STAR★METHODS

KEY RESOURCES TABLE

REAGENT or RESOURCE	SOURCE	IDENTIFIER
Antibodies		
Rabbit Anti-GRP78	Cell Signaling Technology	3183S; RRID:AB_10695864
Rabbit Anti-GADD 153 (R-20)	Santa Cruz Biotechnology	sc-793; RRID:AB_631364
Rabbit Anti-ATF6 α (H-280)	Santa Cruz Biotechnology	sc-22799; RRID:AB_2242950
Rabbit Anti-Phospho-eIF2 α (Ser52)	Santa Cruz Biotechnology	sc-101670; RRID:AB_2096507
Rabbit Anti-Phospho-PERK (Thr981)	Santa Cruz Biotechnology	sc-32577; RRID:AB_2293243
Mouse monoclonal Anti-α-tubulin	Sigma-Aldrich	T5168; RRID:AB_477579
Mouse monoclonal Anti-β-Actin	Sigma-Aldrich	A5316; RRID:AB_476743
Rabbit Anti-Phospho-IRE1 α (Ser724)	Abcam	ab48187; RRID:AB_873899
Rabbit polyclonal Anti-UCP1	Abcam	ab10983; RRID:AB_2241462
Rabbit polyclonal Anti-SPTLC2	Abcam	ab23696; RRID:AB_447617
Rabbit polyclonal Anti-SPTLC1	Abcam	ab84585; RRID:AB_2195858
Bacterial and Virus Strains		
Adenoviral GFP (López et al., 2010; Martínez de Morentin et al., 2014; Martínez-Sánchez et al., 2017a)	Viraquest	N/A
Adenoviral GRP78 (Contreras et al., 2014)	Viraquest	N/A
Adenoviral short hairpin SPTLC1 (In this paper)	Viraquest	N/A
Biological Samples		
Rat tissues		N/A
Chemicals, Peptides, and Recombinant Proteins		
Xylazin hydrochloride	Rompun (Bayer)	N/A
Ketamine (for experiments in University of Santiago, Spain)	Imalgene (Elasa)	N/A
17β-Estradiol	Sigma-Aldrich	E8875
Myriocin	Sigma-Aldrich	M1177
SR59230A hydrochloride	Tocris Bioscience	1511
Dimethyl Sulfoxide (DMSO)	Sigma-Aldrich	D8418
Tauroursodeoxycholic Acid, Sodium Salt	MERCK	580549
N-lauroyl-D-erythro-sphingosine. C12 Ceramide (d18:1/12:0)	Avanti Polar Lipids	860512P
N-palmitoyl-D-erythro-sphingosine C16 Ceramide (d18:1/16:0)	Avanti Polar Lipids	860516P
N-heptadecanoyl-D-erythro-sphingosine C17 Ceramide (d18:1/17:0)	Avanti Polar Lipids	860517
N-stearoyl-D-erythro-sphingosine C18 Ceramide (d18:1/18:0)	Avanti Polar Lipids	860518P
N-lignoceroyl-D-erythro-sphingosine. C24 Ceramide (d18:1/24:0)	Avanti Polar Lipids	860524P
N-nervonoyl-D-erythro-sphingosine. C24:1 Ceramide (d18:1/24:1(15Z))	Avanti Polar Lipids	860525P
Oil Red O solution	Sigma-Aldrich	O1391
Harris' Hematoxylin	Bio-Optica	05-06005/L
Mount Quick Aqueous	Bio-Optica	05-1740
Tri- Sodium Citrate dihydrate	MERCK	A73548612
Ethylene glycol-bis(2-aminoethylether)-N,N,N′,N′-tetraacetic acid (EGTA)	Sigma-Aldrich	E3889-500G
Ethylenediaminetetraacetic acid (EDTA)	Sigma-Aldrich	E9884-500G
Triton X-100	Sigma-Aldrich	X100-500ml
Sodium orthovanadate:	Sigma-Aldrich	S6508-50G
Sodium fluoride	Sigma-Aldrich	S7920-100G

(*Continued on next page*)

Continued

REAGENT or RESOURCE	SOURCE	IDENTIFIER
Sodium pyrophosphate	Sigma-Aldrich	221368-500G
Sucrose	Sigma-Aldrich	S0389
Protease Inhibitor Cocktail Tablets	Roche Dieagnostics	11697498001
Protein Assay Dye Reagent Concentrate (Bradford)	Bio- Rad	500- 0006
30% Acrilamide/ Bis Solution 29:1	Bio- Rad	161- 0156
Experimental Models: Organisms/Strains		
Sprague-Dawley rats (*Rattus norvegicus*)	Animalario Central USC (Spain)	N/A
Software and Algorithms		
FLIR-Tools-Software	FLIR	https://www.flir.com/products/flir-tools/
ImageJ	National Institutes of Health (NIH)	https://imagej.nih.gov/ij/index.html; RRID: SCR_003070
Prism	Graph Pad	https://www.graphpad.com/scientific-software/prism/; RRID: SCR_002798
Other		
Osmotic Minipump	Durect Corporation (Alzet Osmotic Pumps)	Model 2001
Stereotaxic Frame	David Kopf Instruments	Model 900
22-gauge needle	Hamilton	1702N
25-gauge needle	Hamilton	7001N
Polyethylene Tubes (PE20)	Becton Dickinson and Company	427406
Calorimetric System LabMaster	TSE Systems	N/A
B335: Compact-Infrared-Thermal-Imaging-Camera	FLIR	N/A
UPLC/MS	Waters	N/A
Acquity UPLC BEH C8	Waters	186002878
Acquity UPLC BEH C18	Waters	186002350
PVDF transfer membrane	MERCK Millipore	IPVH00010
Olympus XC50	Olympus Corporation	N/A
Olympus IX51	Olympus Corporation	N/A
EcoMRI 700: Body Composition Analyzer	EcoMRI	Model 700
Cryostat	Leica Biosystems	CM 1850 UV
Lock Spray Mass Ionization Source	Waters	N/A
Medical X- Ray Film	Fujifilm	47410 19289

CONTACT FOR REAGENT AND RESOURCE SHARING

Further information and request for resources and reagents should be directed to and will be fulfilled by the Lead Contact, Miguel López (m.lopez@usc.es).

EXPERIMENTAL MODEL AND SUBJECT DETAILS

Animals and housing conditions

Adult female Sprague-Dawley rats (250–300 g; *Animalario General USC*; Santiago de Compostela, Spain) were used for the experiments. The experiments were performed in agreement with the *International Law on Animal Experimentation* and were approved by the *USC Ethical Committee (Project ID 15010/14/006).* The animals were housed with an artificial 12-hour light (8:00 to 20:00)/12-hour dark cycle, under controlled temperature and humidity conditions and allowed to free access to standard laboratory chow and tap water. For all the procedures, the animals were caged individually, but for OVX recovery time the rats were housed in groups (4 rats/cage). During this post-operative recovery period the animals became accustomed to the handling procedure under non-stressful conditions.

METHOD DETAILS

Ovariectomy

Rats were bilaterally ovariectomized (OVX) or Sham-operated as described previously (Martínez de Morentin et al., 2014, 2015). Briefly, under ketamine–xylazine anesthesia (50 mg/kg, intraperitoneal, IP) both flanks were shaved, and rats were placed on their left flank. Then, an incision was made in the right flank skin and muscle layers. The ovary was then carefully pulled out. The distal part of uterine horn was ligated with surgical suture and then the ovary was removed after making a dissection between the suture and the ovary. After returning the horn into the abdominal cavity, the wound was closed suturing the muscle layer with surgical silk and applying surgical staples to the skin. The same procedure was applied to remove the left ovary. Sham surgeries were also performed, in which each ovary was exposed but not tied or dissected. All treatments (central or peripheral) on OVX rats were carried out two weeks after surgery to ensure a total washout of ovarian hormones, as previously reported (Martínez de Morentin et al., 2014, 2015).

Central and peripheral treatments

For the central estradiol experiments, intracerebroventricular (ICV) cannulae were stereotaxically implanted under ketamine/xylazine anesthesia, as previously described using the following coordinates 1.6 mm lateral to bregma, 0.6 mm posterior, 4.5 mm deep (López et al., 2008, 2010; Whittle et al., 2012; Martínez de Morentin et al., 2012, 2014, 2015; Contreras et al., 2014, 2017; Martins et al., 2016; Martínez-Sánchez et al., 2017a; Seoane-Collazo et al., 2018). Animals were individually housed and used for experimentation four days later. Then, rats were subjected to a protocol of daily ICV injections of estradiol (17 β-estradiol; 1 nmol dissolved in 5 μL of saline containing 10% of DMSO; *Sigma;* St Louis, MO, USA) or vehicle (5 μL of saline containing 10% of DMSO; control rats) using a 22-gauge needle (*Hamilton;* Reno, NV, USA) through the inserted cannulae at 8:00 and 20:00 for 6 days (Martínez de Morentin et al., 2014, 2015).

For the central treatment with myriocin or tauroursodeoxycholic acid (TUDCA), ICV cannulae were stereotaxically implanted under ketamine/xylazine anesthesia, as previously described and a catheter tube was connected from the cannulae to an osmotic mini-pump flow moderator (*model 2001*; *Alzet Osmotic Pumps*; Palo Alto, CA, USA) (Martins et al., 2016; Contreras et al., 2017), during the same surgery procedure. The minipump was inserted in a subcutaneous pocket on the dorsal surface of the animal, created using blunt dissection. The incision was closed. The rats were then infused with the serine palmitoyltransferase inhibitor, myriocin (4 μg/day dissolved in saline containing 1/3 of DMSO; *Sigma*; St Louis, MO, USA) or the chemical chaperone TUDCA (10 μg/day dissolved in PBS; *Calbiochem, Billerica*; MA, USA) or their respective vehicle (saline containing 1/3 of DMSO or PBS; control rats) for 6 days. The selection of these doses was based on previous reports (Ramírez et al., 2013; Contreras et al., 2017). Finally, the β3-AR specific antagonist SR59230A ([3-(2ethylphenoxy)-1-[(1,S)-1,2,3,4-tetrahydronapth-1-ylamino]-2S-2-propanol-oxalate] (3 mg/Kg/day dissolved in DMSO; *Tocris Bioscience;* Bristol, UK) (López et al., 2010; Martínez de Morentin et al., 2014; Contreras et al., 2014, 2017; Martínez-Sánchez et al., 2017a; Seoane-Collazo et al., 2018) was administrated subcutaneously twice a day at the onset of the cycles at 8:00 and 20:00, starting 2 days before the first ICV and stereotactic injections.

Stereotaxic microinjection of adenoviral vectors

Rats were placed in a stereotaxic frame (*David Kopf Instruments*; Tujunga, CA, USA) under ketamine/xylazine anesthesia. The VMH was targeted bilaterally using a 25-gauge needle (*Hamilton;* Reno, NV, USA). The injections were directed to the following stereotaxic coordinates: 2.4/3.2 mm posterior to the bregma (two injections were performed in each VMH), ± 0.6 mm lateral to midline and 10.1 mm ventral, as previously reported (López et al., 2008, 2010; Whittle et al., 2012; Martínez de Morentin et al., 2012, 2014, 2015; Contreras et al., 2014, 2017; Martins et al., 2016; Martínez-Sánchez et al., 2017a, b; Seoane-Collazo et al., 2018). Adenoviral vectors (*Viraquest;* North Liberty, IA, USA) containing green fluorescence protein (GFP, used as control), GRP78 (at 10^{12} pts/mL), short hairpin serine palmitoyltransferase long chain subunit 1 (shSPTLC1, at $1.1x10^{12}$ pts/mL) were delivered at a rate of 200 nL/min for 5 min (1 μL/injection site) as previously reported (López et al., 2008, 2010; Whittle et al., 2012; Martínez de Morentin et al., 2012, 2014, 2015; Contreras et al., 2014, 2017; Martins et al., 2016; Martínez-Sánchez et al., 2017a, b; Seoane-Collazo et al., 2018).

Temperature measurements

Body temperature was recorded twice at the end of the treatments with a rectal probe connected to a digital thermometer (*BAT-12: Microprobe-Thermometer; Physitemp*; NJ, US). Skin temperature surrounding BAT was recorded with an infrared camera (*B335:Compact-Infrared-Thermal-Imaging-Camera; FLIR;* West Malling, Kent, UK) and analyzed with a specific software package (*FLIR-Tools-Software; FLIR;* West Malling, Kent, UK) (Whittle et al., 2012; Martínez de Morentin et al., 2012, 2014, 2015; Contreras et al., 2014, 2017; Martins et al., 2016; Martínez-Sánchez et al., 2017a; Seoane-Collazo et al., 2018).

Calorimetric system and nuclear magnetic resonance

Animals were analyzed for EE using a calorimetric system (*LabMaster; TSE Systems*; Bad Homburg, Germany). Animals were placed in a temperature-controlled (24°C) box through which air was pumped. After calibrating the system with the reference gases (20.9% O_2, 0.05% CO_2 and 79.05% N_2), the metabolic rate was measured for 3 days, as previously shown (Imbernon et al., 2013; Martínez de Morentin et al., 2012, 2014; Martins et al., 2016; Martínez-Sánchez et al., 2017a; Seoane-Collazo et al., 2018). EE were recorded

every 30 min. Animals were placed for adaptation for 1 week before starting the measurements. For the measurement of body composition, we used nuclear magnetic resonance (NMR) (*Whole Body Composition Analyzer; EchoMRI*; Houston, TX) (Imbernon et al., 2013; Martínez de Morentin et al., 2012, 2014; Martins et al., 2016; Martínez-Sánchez et al., 2017a; Seoane-Collazo et al., 2018). Animals do not need to be anesthetized neither other special preparation before measurement. They are placed in a holder of custom-defined size during the measurement (measuring time: 0.5-3.2 min). Two measurements were done twice for animal 72 h apart.

Sample processing

Rats were killed by cervical dislocation and decapitation. From each animal, the MBH, VMH, liver and the interscapular BAT were collected for western blotting and Oil Red O staining and immediately homogenized on ice to preserve phosphorylated protein levels. Those samples and the serum were stored at −80°C until further processing. Dissection of the VMH was performed by micro-punch procedure under the microscope, as previously described (López et al., 2010; Whittle et al., 2012; Contreras et al., 2014, 2017; Martínez de Morentin et al., 2014; Martins et al., 2016; Martínez-Sánchez et al., 2017a; Seoane-Collazo et al., 2018).

Ceramide quantification

Ceramide analysis reported in this manuscript were performed in two different laboratories and according to the next methods. In the first one, ceramides were extracted and analyzed using liquid chromatography-mass spectrometer consisted of a *Waters* Acquity UPLC System connected to a *Waters* LCT Premier Orthogonal Accelerated Time of Flight Mass Spectrometer (*Waters*; Millford, MA, USA), operated in positive electrospray ionization mode. Full scan spectra from 50 to 1500 Da were acquired and individual spectra were summed to produce data points each 0.2 s. Mass accuracy and reproducibility were maintained by using an independent reference spray by the LockSpray interference. The analytical column was a 100 mmL 2.1 mm i.d., 1.7 mm C8 Acquity UPLC BEH (*Waters*; Millford, MA, USA). The two mobile phases were phase A: methanol; phase B: water, both contained 0.2% formic acid (v/v) and 2 mM ammonium formate. A linear gradient was programmed (0.0 min: 20% B; 3 min: 10% B; 6 min: 10% B; 15min: 1% B; 18 min: 1% B; 20 min: 20% B; 22 min: 20% B). The flow rate was 0.3 mL/min. The column was held at 30°C. Quantification was carried out using the extracted ion chromatogram of each compound, using 50 mDa windows. The linear dynamic range was determined by injecting standard mixtures. Positive identification of compounds was based on the accurate mass measurement with an error < 5 ppm and its LC retention time, compared to that of a standard (±2%). Concentrations were measured by multiple reaction monitoring experiments using N-lauroyl-D-erythro-sphingosine (C12-ceramide) and N-Heptadecanoyl-D-erytro-Sphingosine (C17-ceramide) as internal standards and using as patrons N-Palmitoyl-D-erytro-sphingosine (C16-ceramide), N-Stearoyl-D-erytro-sphingosine (C18-ceramide), N-lignoceroyl-D-erythro-sphingosine (C24-ceramide) and N-nervonoyl-D-erythro-sphingosine (C24:1-ceramide) (*Avanti Polar Lipids*; Alabaster, AL, USA). The ceramide analyses from Figure 1K were performed in the *Research Unit on Bioactive Molecules* (*RUBAM*) of the Institut de Química Avançada de Catalunya (IQAC-CSIC) according to this method.

In the second one, total lipid species were extracted according to the method of Folch et al. (1957). Ceramide lipid species were enriched in the lower phase (organic phase) and analyzed using an untargeted lipidomic approach by liquid chromatography coupled with high-resolution mass spectrometry (LC–HRMS) as described by Seyer et al. (2016). The ceramide analyses from Figure 1F were performed in the *Unité de Biologie Fonctionnelle et Adaptative* (Univertsité Paris Diderot) according to this method.

Histological analyses

Hepatic lipid content was analyzed by Oil Red O staining, as previously shown (Seoane-Collazo et al., 2014; Contreras et al., 2014, 2017; Imbernon et al., 2016; Porteiro et al., 2017; Martínez-Sánchez et al., 2017a). Hepatic frozen sections were cut (8 μm) and fixed in 10% buffered formaldehyde. Sections were stained in filtered Oil Red O (*Sigma*; St. Louis, MO, USA), washed in distilled water, counterstained with Harris hematoxylin (*Bio-Optica*; Milan, Italy) and washed in distilled water again. Sections were mounted in aqueous mounting medium (*Bio-Optica;* Milan, Italy). Images were taken with a digital camera *Olympus XC50* (*Olympus Corporation*; Tokyo, Japan) at 20X. Digital images of liver were quantified with *ImageJ Software* (*National Institutes of Health*; USA). Direct detection of GFP fluorescence was performed after perfusion of the animals; on 40 μm brain sections. Images were taken with a fluorescence microscope *Olympus IX51*, as previously shown (Contreras et al., 2017; Seoane-Collazo et al., 2018).

Western blotting

Protein lysates from hypothalamus (MBH or VMH) and BAT were homogenized in lysis buffer (consisting of a mix of 0.05 M Tris-HCl, 0.01 M EGTA, 0.001 M EDTA, 0.016 M Triton X-100, 0.001 M sodium orthovanadate, 0.05 M sodium fluoride, 0.01 M sodium pyrophosphate and 0.25 M sucrose, made up with distilled water and adjusted to 7.5 pH; all of them from *Sigma*; St. Louis, MO, USA) and freshly added protease inhibitor cocktail tablets (*Roche Diagnostics*; Indianapolis, IN, USA). The protein concentration was determined by the *Bradford Method* (Protein assay dye concentrate, *Bio-Rad Laboratories*; Hercules, CA, USA), and the total protein content of the tissues was calculated. The protein lysates were subjected to SDS-PAGE, electrotransferred to polyvinylidene difluoride membranes (PVDF; *Millipore*; Billerica, MA, USA) with a semidry blotter and probed with antibodies against GRP78 (*Cell Signaling*; Danvers; MA, USA); ATF6α, CHOP, peIF2α (Ser52), pPERK (Thr981) (*Santa Cruz*; Santa Cruz, CA,USC); pIREα (Ser724), SPTLC1, SPTLC2, UCP1 (*Abcam*; Cambridge, UK); α-tubulin or β-actin (*Sigma*; St. Louis, MO, USA) as described (López et al., 2010; Varela et al., 2012; Martínez de Morentin et al., 2014; Contreras et al., 2014; Martínez-Sánchez et al., 2017a; Seoane-Collazo et al., 2018).

Each membrane was then incubated with the corresponding secondary antibody: anti-mouse or anti-rabbit (all of them from *DAKO*; Glostrup, Denmark). The membranes were exposed to an X-ray film (*Fujifilm*; Tokyo, Japan) and developed using developer (*Developer G150; AGFA HealthCare*: Mortsel, Belgium) and Fixator (*Manual Fixing G354; AGFA HealthCare*: Mortsel, Belgium).

Autoradiographic films were scanned and the bands signal was quantified by densitometry using *ImageJ-1.33 software* (*NIH*; Bethesda, MD, USA). Values were expressed in relation to β-actin (hypothalamus) or α-tubulin (BAT). Representative images for all proteins are shown; in the case of the loading controls a representative gel is displayed for clarity, although each band of each protein was always corrected by its own internal control band (β-actin or α-tubulin). In all the Figures showing images of gels, all the bands for each picture come always from the same gel, although they may be spliced for clarity.

QUANTIFICATION AND STATISTICAL ANALYSIS

ImageJ-1.33 software (*NIH*; Bethesda, MD, USA) was used to process western blot analyses and liver histologic images (López et al., 2010; Varela et al., 2012; Martínez de Morentin et al., 2014; Contreras et al., 2014; Martínez-Sánchez et al., 2017a, b; Seoane-Collazo et al., 2018). *FLIR-Tools-Software; FLIR;* West Malling, Kent, UK) was used to process the thermal images (Whittle et al., 2012; Martínez de Morentin et al., 2012; Contreras et al., 2014, 2017; Martínez de Morentin et al., 2014, 2015; Martins et al., 2016; Martínez-Sánchez et al., 2017a; Seoane-Collazo et al., 2018). Statistical analysis was conducted using *GraphPad Prism 6 Software* (*GraphPad Software, Inc.*; La Jolla, CA, USA). Data are expressed as mean ± SEM. Protein data were expressed in relation (%) to control (Sham or OVX, vehicle or GFP treated) rats. Error bars represent SEM. Statistical significance was determined by Student's t test (when two groups were compared) or ANOVA (when more than two groups were compared) followed by post hoc Bonferroni test. $p < 0.05$ was considered significant. The number of animals used in each experimental setting and analysis are specified in each figure legend.